Journal of Applied Research and Technology

www.jart.icat.unam.mx

Journal of Applied Research and Technology 21 (2023) 526-534

Original

Model identification and $\mathcal{H}_\infty$ control of an aeropendulum

Ricardo Breganon[a,b]* • Uiliam Nelson L. T. Alves[a,b] • João Paulo L. S. de Almeida[a] • Fernando S. F. Ribeiro[a] • Marcio Mendonça[b] • Rodrigo H. C. Palácios[b] • Marcio A. F. Montezuma[b]

[a]*IFPR – Instituto Federal do Paraná, Jacarezinho – PR, Brazil*
[b]*UTFPR – Universidade Tecnológica Federal do Paraná, Cornélio Procópio – PR, Brazil*

Received 12 01 2021; accepted 09 26 2022
Available 08 31 2023

Abstract: The aeropendulum is a nonlinear system that consists of a rod equipped with a motorized propeller at one of its ends and connected to a pivot at its other end. This pivot receives a torsional moment through the aerodynamic effects generated by the propeller thrust force. From a control point of view, the aeropendulum is a plant that imposes a significant complexity on the design of controllers. In view of that, this system can be used in didactic observations and real applications of control theory concepts. This work presents the model identification and $\mathcal{H}_\infty$ control of an aeropendulum system prototype. The model has as control input the voltage applied to the motor that drives the propeller and the rod angle as system output, measured by an incremental encoder. The identification process was conducted using the ident function of the Matlab® software. Based on the obtained model, an $\mathcal{H}_\infty$ controller was designed to stabilize the system around the operating point, maintaining the rod in a specific position. A square wave was used as a reference for the angular variation of the rod to verify the controller's efficiency in tracking a required angular trajectory. Simulation and experimental tests were conducted to validate the obtained mathematical model and the controller design. The results confirmed that the considered methodology was satisfactory for the studied case.

Keywords: Aeropendulum, model identification. $\mathcal{H}_\infty$ control

*Corresponding author.
E-mail address: ricardo.breganon@ifpr.edu.br (Ricardo Breganon).
Peer Review under the responsibility of Universidad Nacional Autónoma de México.

1. Introduction

Stability problems can be studied in different pendulum systems. The aeropendulum, for example, consists of a rod equipped with a motorized propeller at one of its ends, whereas the other end is connected to a pivot point. The rod moves by the aerodynamic effect created by the thrust force of the propeller, which must be actuated according to the desired position for the rod angle (Baskoro & Kurniawan, 2020). From the perspective of the control area, the aeropendulum is a nonlinear system and can be controlled by classical control techniques when the system is linearized around the operating point (Job & Jose, 2015; Prasetyo & Endryansyah, 2020; Yoon, 2016). Furthermore, in the literature, the aeropendulum is also considered a simplified model of an unmanned autonomous vehicle and can be used for teaching dynamic systems and control techniques in engineering education (Enikov & Campa, 2012; Taskin, 2017).

Some examples of control approaches in aeropendulum systems are presented below: a PID controller applied to a pendulum driven by propellers is discussed in the paper of Mohammadbagheri and Yaghoobi (2011). Job and Jose (2015) present the mathematical modelling of an aeropendulum system and compare stability and position control between a PID, LQR and PID controller based on LQR. A Fuzzy PID controller is proposed by Taskin (2017) for the angular position control of an aeropendulum system. An observer-based Fuzzy LMI regulator is used for stabilization and tracking control of an aeropendulum (Farooq et al., 2015). Tengis and Batmunkh (2018) developed a supervised machine learning algorithm for controlling an aeropendulum. A digital PD controller and an act-and-wait controller are shown in Habib et al. (2017). Rodrigues et al. (2021) present tuning rules for a simplified dead-time compensator to control the angular position of an aeropendulum.

In particular, the $\mathcal{H}_\infty$ controller is also a valid option in pendulum system applications, as shown in the following works, which discuss: the stabilization of the wheeled inverted pendulum (Rigatos et al., 2020; Thanh et al., 2019), and of a Furuta pendulum (Rigatos et al., 2018); position and orientation control on a Stewart platform (Breganon et al., 2018); the stability control of a 2-degree-of-freedom quadrotor (Sampaio et al., 2011); and the position analysis of a brushless motor (Hans & Ghosh, 2020), component commonly used in aeropendulum systems; among others.

Based on the aforementioned, this work presents a modelling and control methodology for an experimental aeropendulum system. First, the model is obtained by identifying the plant around an operating point, using the *ident* tool of the Matlab®. Then, the control strategy is employed to stabilize the system close to a desired operating point. The aeropendulum prototype considered in this work is part of the Automation Laboratory of the Federal Institute of Paraná, Jacarezinho, Paraná, Brazil and was developed in partnership with the Federal Technological University of Paraná, Cornélio Procópio, Paraná, Brazil.

The rest of the paper is divided as follows: In Section 2, an overview of the aeropendulum prototype and the identification of its mathematical model are presented; in Section 3, the design of the $\mathcal{H}_\infty$ controller is described; results and discussions are presented in Section 4; and the conclusions, in Section 5.

2. Aeropendulum prototype and identification of its mathematical model

This work considered the aeropendulum prototype shown in Figure 1. The main components that constitute this prototype are listed in Table 1.

The propeller, coupled to the brushless motor, is responsible for generating the thrust necessary for the movement in the system, enabling the angular variation of the rod. A speed control signal drives the motor, and an encoder measures the angular position of the rod. The speed control drive and encoder are connected to a data acquisition board from the National Instruments® manufacturer, PCI-6602 model, used by an Intel Core 2 Duo E8600 3.33 GHz computer with 2 GB of RAM. The computer supports the Matlab/Simulink® software used to develop the methodology presented in this work.

Table 1. Aeropendulum component list.

Number	Item	Description
01	Aluminum rod	6.35 mm in diameter, 400 mm in length
01	Brushless motor	Model: Mystery F2836, 3800 V/RPM
01	Battery	LiPo 11.1V
01	Propeller	203.2 mm with pitch 5
01	Electronic speed control	Imax = 40 A
01	Encoder	Type: incremental 600 PPR

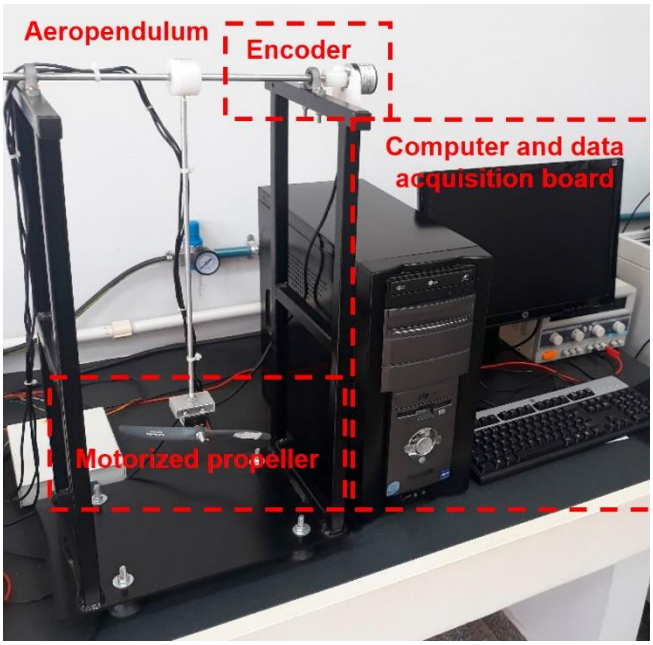

Figure 1. Aeropendulum prototype available at the Automation Laboratory of the Federal Institute of Paraná, Jacarezinho.

By considering the torque generated by the thrust of the propeller ($\tau(t)$) as the input of the system and the angle of the rod ($\theta(t)$) as a variable of interest, the aeropendulum system can be described by a second-order nonlinear dynamics given by

$$J\ddot{\theta}(t) = -(m_1 l_1 + m_2 l_2) g \sin\big(\theta(t)\big) - b\dot{\theta}(t) + \tau(t), \quad (1)$$

where J is the total moment of inertia of the mobile parts of the system, m_1 and m_2 are the mass of the rod and motor+propeller set, respectively, l_1 and l_2 are the distances between the centers of mass of the rod and the motor+propeller set to the rotational pivot of the system, respectively, g is the acceleration of gravity, and b, the viscous friction coefficient of the rotational pivot (Enikov & Campa, 2012; Farooq et al., 2015; Job & Jose, 2015; Khoirudin & Endryansyah, 2020; Taskin, 2017).

Let the operating point of the aeropendulum be given by (θ_0, τ_0), where θ_0 is the angle of the rod at the operating point, and τ_0, the torque that produces the angle θ_0. So, it's possible to linearize Eq. 1 around this point, resulting in the transfer function given by

$$\frac{\Delta\Theta(s)}{\Delta T_r(s)} = \frac{k_1}{s^2 + k_2 s + k_3}, \quad (2)$$

in which $\Delta\Theta(s)$ is the Laplace transform of the rod angle variation: $\Delta\theta(t) = \theta(t) - \theta_0$, $\Delta T_r(s)$ is the Laplace transform of the torque variation: $\Delta\tau(t) = \tau(t) - \tau_0$, and k_1, k_2 and k_3 are constant coefficients that depend on the operation point (θ_0, τ_0).

In this work, the voltage applied to the motor is the input of the model. Thus, the relationship between the applied voltage and the torque in the rotational pivot must be considered. This relationship was considered as a first-order dynamic, represented by

$$\frac{\Delta T_r(s)}{\Delta U(s)} = \frac{k_4}{s + k_5}, \quad (3)$$

where $\Delta U(s)$ is the Laplace transform of the voltage variation, $\Delta u(t) = u(t) - u_0$, applied to the motor, and u_0 is the voltage producing the torque τ_0.

Note that the dynamics between voltage and rod angle is given by a third-order transfer function (Eq. 2 and Eq. 3 in series). As shown in the following subsection, this model proved to be adequate for the data collected in the identification process.

2.1. Identification process

In order to establish a linear mathematical model for the aeropendulum system shown in Figure 1, an identification process was performed using the *ident* tool from Matlab®. The obtained model was used in the design of the $\mathcal{H}_\infty$ controller for the system and to perform simulations.

A test was conducted in the prototype to collect the experimental data used to identify the mathematical model. Initially, a step signal of amplitude $u_0 = 1.3$ V was applied to the system input. This input caused the aeropendulum rod's movement from the rest condition (rod pointed downwards) to the operation angle $\theta_0 = 1.1$ rad. This angle and voltage were considered the operation point for the experiment. After the system stabilized in the operation point, a step signal of $\Delta u(t) = 0.3$ V was added to the system's input. This additional signal played the role of input in the model of Eq. 3. Along with the $u(t)$ signal, the evolution of the system output $\theta(t)$ was also recorded. Then, the angle variation was obtained using $\Delta\theta(t) = \theta(t) - \theta_0$.

After that, the ident function of Matlab® was used. The input signal was the step increment $\Delta u(t)$, while the output was the response angle variation $\Delta\theta(t)$. Finally, a third-order model was chosen for the transfer function, resulting in the transfer function shown in Eq. 4. This model fits the data collected in the real system in 83.58%. Figure 2 shows the prototype and simulated responses based on the system model and amplitude step input $\Delta u(t) = 0.3$ V.

$$\frac{\Delta\Theta(s)}{\Delta U(s)} = \frac{30.82}{s^3 + 3.044s^2 + 17.84s + 43.54} \quad (4)$$

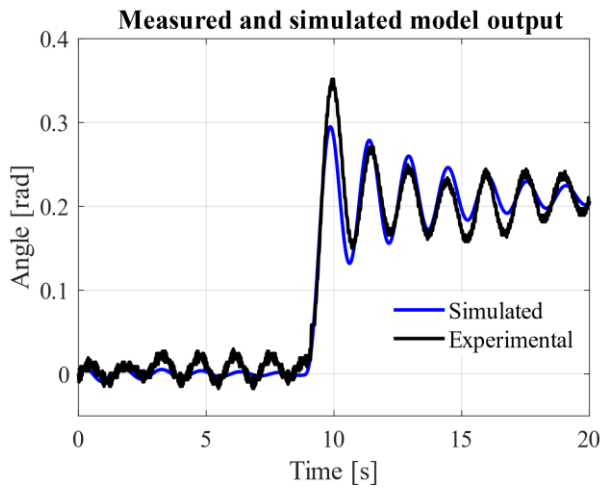

Figure 2. Step response of the aeropendulum prototype (Experimental) and step response of the model given by Eq. 4 (Simulated).

3. $\mathcal{H}_\infty$ Control design

The standard $\mathcal{H}_\infty$ control problem is formulated to find a controller $K(s)$ such that the closed-loop system is stable and keeps the desired performance. First, consider the diagram of a SISO feedback system, shown in Figure 3 (Doyle et al., 1989; Oliveira et al., 2017; Zhou et al.,1995).

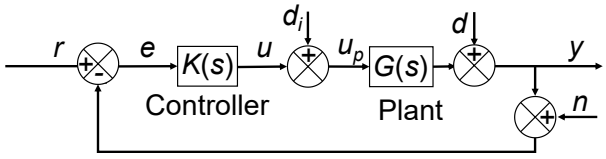

Figure 3. Typical diagram of a feedback system (adapted from Oliveira et al., 2017).

From the feedback diagram represented in Figure 3, we obtain

$$e = r - y = S(r - d) + Tn + SGd_i, \tag{5}$$

$$u = KS(r - n - d) + Sd_i, \tag{6}$$

where d_i is the plant's input disturbance, d is the output disturbance, and n represents the sensor's noises. In Eqs. 5 and 6, the sensitivity function $S(s)$ and the complementary sensitivity function $T(s)$ are given by

$$S(s) = \left(I + G(s)\,K(s)\right)^{-1} \tag{7}$$

$$\begin{aligned} T(s) &= G(s)K(s)\left(I + G(s)\,K(s)\right)^{-1} \\ &= I - S(s). \end{aligned} \tag{8}$$

From Eq. 5, for e to be small compared to the disturbances d and d_i, and the reference signal r, $S(s)$ must be small. On the other hand, $T(s)$ must be small to obtain a small effect of the noise n on the error e. However, $T(s) + S(s) = I$ and then it is impossible to simultaneously reach both of the mentioned objectives at the same frequency range. Another critical point in the controller design is the magnitude of the control signal u, which must be small in order to stay within the physical constraints of the system (within the saturation limits). From Eq. 6, this can be achieved if, in addition to $S(s)$, $K(s)S(s)$ has a small amplitude. In these discussions, the size of the complex functions is understood through its $\mathcal{H}_\infty$ norm, which is defined as

$$\|S\|_\infty = \sup_\omega |S(j\omega)|. \tag{9}$$

Thus, specifications for attenuation of disturbance and steady-state error can be defined by means of an upper bound limit of the norm of $S(j\omega)$, defined in Eq. 9, that is

$$|S(j\omega)| \leq |W_1^{-1}(j\omega)|, \forall\, \omega, \tag{10}$$

where $W_1(j\omega)$ ponders $S(j\omega)$ and reflects the desired attenuation for each frequency ω.

From Eq. 6, a constraint on the control signal u can be introduced by a bound on $K(j\omega)\,S(j\omega)$, which can be achieved by imposing

$$|K(j\omega)\,S(j\omega)| \leq |W_2^{-1}(j\omega)|, \forall\, \omega, \tag{11}$$

such that the function $W_2(j\omega)$ limits the control input within an acceptable range, avoiding the saturation.

In order to guarantee the robust stability of the system, an upper bound of the complementary sensitivity function can be specified by

$$|T(j\omega)| \leq |W_3^{-1}(j\omega)|, \forall\, \omega, \tag{12}$$

where the function $W_3(j\omega)$ minimizes the peak of $T(s)$, so that oscillations are mitigated and stability is guaranteed (Oliveira et al., 2017). However, $W_3(j\omega)$ and $W_1(j\omega)$ conflict, especially at low frequencies, due to the relation $S(s) + T(s) = I$.

The constraints described by Eqs. 10, 11 and 12 can be understood as a restriction in the $\mathcal{H}_\infty$ norm of an augmented plant based on the diagram of Figure 3. The augmented plant with the weighting functions is presented in Figure 4, in which

w and u are the augmented system's inputs, z_1, z_2, z_3 are the outputs, and e is the error. In this diagram, w and u correspond to the reference r and the control signal u defined in Figure 3, respectively.

From the diagram of Figure 4, considering the output vector $z = [z_1 \quad z_2 \quad z_3]^T$ and the input w, the transfer function matrix T_{zw} is given by Eq. 13.

$$T_{zw} = \begin{bmatrix} W_1 S \\ W_2 KS \\ W_3 T \end{bmatrix}. \tag{13}$$

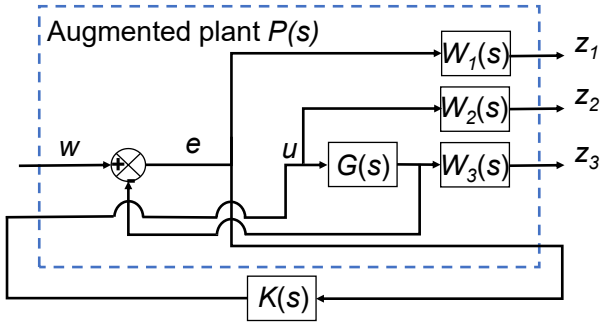

Figure 4. Augmented plant for the $\mathcal{H}_\infty$ control design (adapted from Oliveira et al., 2017).

The norm constraints defined in Eqs. 10, 11 and 12 can be described by means of a bound in the $\mathcal{H}_\infty$ norm of T_{zw} (Eq. 13):

$$\|T_{zw}\|_\infty = \left\| \begin{matrix} W_1 S \\ W_2 KS \\ W_3 T \end{matrix} \right\|_\infty \leq \gamma. \tag{14}$$

Understanding the effects of the weighting functions $W_1(j\omega)$, $W_2(j\omega)$, and $W_3(j\omega)$ on the control system is crucial for modeling the specifications according to the desired response characteristics of the system. In view of this, the following weighting functions were adopted to minimize the steady-state error, restrict the control input, and ensure stability:

$$W_1(s) = \frac{2.25}{s + 0.00025} \tag{15}$$

$$W_2(s) = \frac{4.5}{50} \tag{16}$$

$$W_3(s) = \frac{100s + 20}{s + 500}. \tag{17}$$

The $\mathcal{H}_\infty$ controller for the aeropendulum was designed using the function *hinf* of Matlab®, the model of Eq. 4, and the weighting functions from Eqs. 15, 16, and 17. The resulted controller is described in state space by

$$\begin{aligned} \dot{x} &= A_c x + B_c e \\ u &= C_c x + D_c e, \end{aligned} \tag{18}$$

where

$$A_c = \begin{bmatrix} -4.58 & 4.58 & -7.34 & 19.63 & -0.33 \\ -2.81 & -2.39 & 2.95 & -6.21 & 0.11 \\ 1.31 & 1.35 & -3.88 & 15.57 & -0.26 \\ 0.85 & 6.46 & -2.42 & -14.4 & 0.21 \\ 0 & 0 & 0 & 0.0003 & -500 \end{bmatrix}$$

$$B_c = \begin{bmatrix} 0.567 \\ -3.143 \\ -9.104 \\ -45.752 \\ 0.0001 \end{bmatrix} \tag{19}$$

$$C_c = [0.314 \quad -0.504 \quad 0.683 \quad -2.713 \quad 0.046]$$

$$D_c = [0].$$

Figures 5, 6, and 7 show the Bode diagram of $S(j\omega)$ (Eq. 7), $K(j\omega)S(j\omega)$, and $T(j\omega)$ (Eq. 8) for the controller given in Eqs. 18 and 19, the plant in Eq. 4, and the inverse of the weighting functions in Eqs. 15, 16 and 17. It is possible to notice that the constraints in Eqs. 10, 11, and 12 were satisfied by the designed controller.

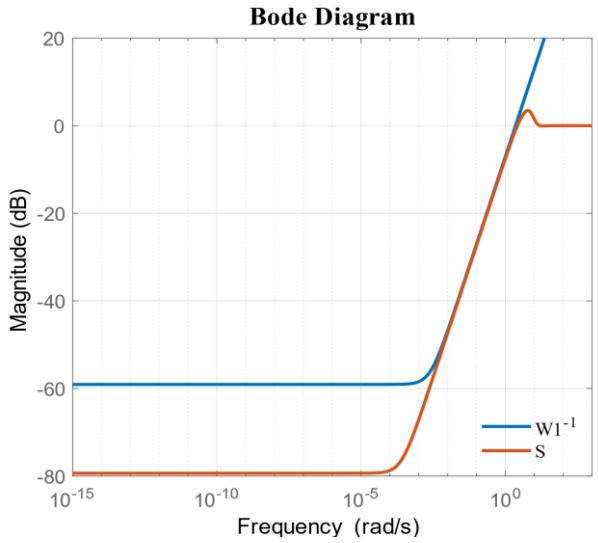

Figure 5. Bode diagram of the sensitivity function $S(j\omega)$ (Eq. 7) for the closed-loop plant Eq. 4 with the controller in Eqs. 18 and 19, and the inverse of $W_1(s)$ in Eq. 15.

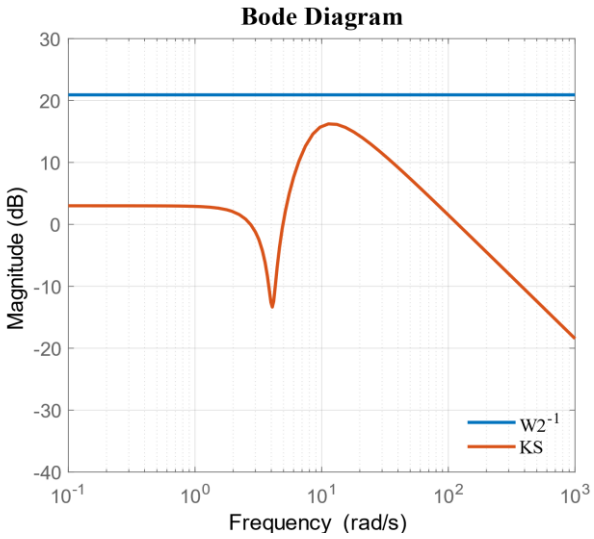

Figure 6. Bode diagram of $K(j\omega)S(j\omega)$ for the closed-loop plant Eq. 4 with the controller in Eqs. 18 and 19, and the inverse of $W_2(s)$ in Eq. 16.

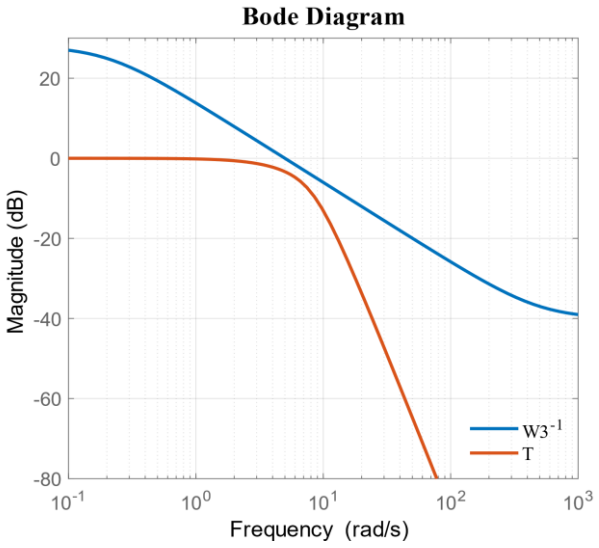

Figure 7. Bode diagram of the complementary sensitivity function $T(j\omega)$ (Eq. 8) for the closed-loop plant Eq. 4 with the controller in Eqs. 18 and 19, and the inverse of $W_3(s)$ in Eq. 17.

4. Results and discussions

Based on the identification and design methodology of the $\mathcal{H}_\infty$ controller, steps presented in Sections 2 and 3, respectively, experiments were carried out to validate the proposal of this work through simulation and tests with the real aeropendulum. Thus, the aeropendulum prototype shown in Figure 1 and the block diagram shown in Figure 3 were considered for the operating point (θ_0,u_0). The resulting control structure is shown in Figure 8, where y corresponds to the angle of the rod in the aeropendulum.

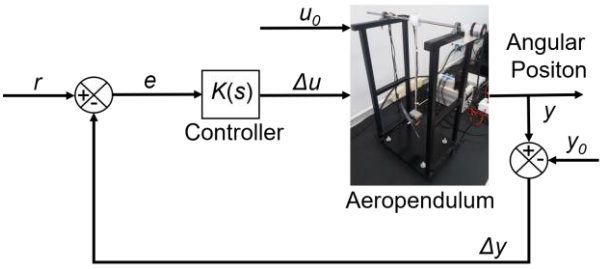

Figure 8. Block diagram of the closed-loop aeropendulum working around an operation point.

A square wave with 0.26 rad of amplitude, period of 20 s, and pulse width of 50% was applied as a reference input for $\Delta\theta(t)$ in the aeropendulum system (simulation and real prototype). The simulation used the model in Eq. 4, and both simulation and bench experiment used the controller in Eqs. 18 and 19 and the control diagram in Figure 8. The results allowed validating the model, which was carried out through the identification, and the design of the $\mathcal{H}_\infty$ controller. Figures 9, 10, and 11 show the obtained results.

One can observe in Figure 9 that the system output (rod angle variation) has an oscillatory characteristic in the real system result. However, the rise time in the simulation and the experimental are similar. This similarity between the results is due to the fit of the model with the data from the real plant, which is 83.58%, as mentioned in Section 2.

In Figure 10, the system error is shown for both simulation and experimental tests. In both cases, the $\mathcal{H}_\infty$ controller acted to tend the error to zero, ensuring the system's stability and the tracking of the reference.

Figure 11 shows the control signal in simulation and experimental tests, which were satisfactory in stabilizing the system and maintain the system output following the square wave reference. Furthermore, it is possible to observe that the simulation and experimental plant's control signal presented similar characteristic.

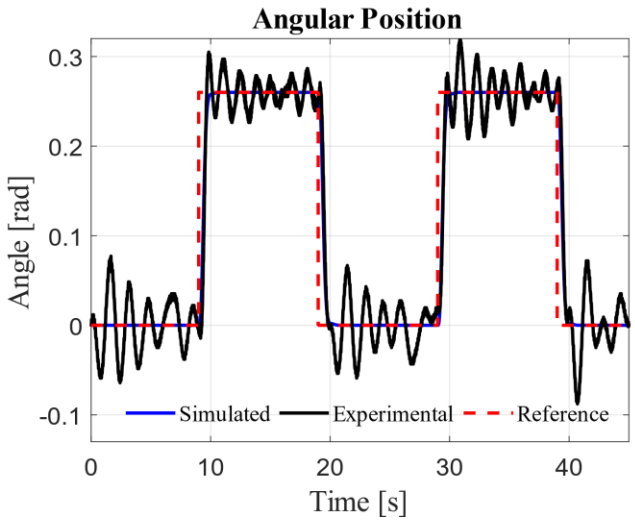

Figure 9. Angular variation of the aeropendulum rod $\Delta\theta(t)$ around the operation point in simulation (Simulated) and experimental tests (Experimental), and its reference (Reference).

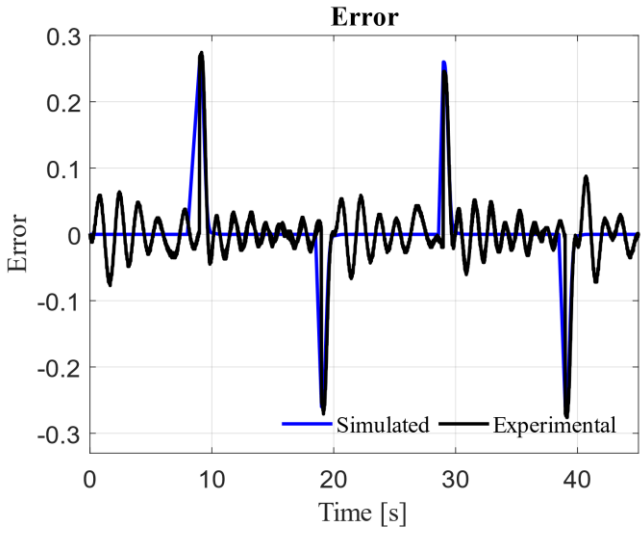

Figure 10. Error between angular variation of the aeropendulum rod around operation point and its reference in simulation (Simulated) and in experimental tests (Experimental).

5. Conclusions

This work presented the model identification, $\mathcal{H}_\infty$ controller design, and experimental tests of an aeropendulum system prototype. The model obtained is linear and valid around an operating point, and the controller aimed to stabilize the system in the operation point and track a reference around this point.

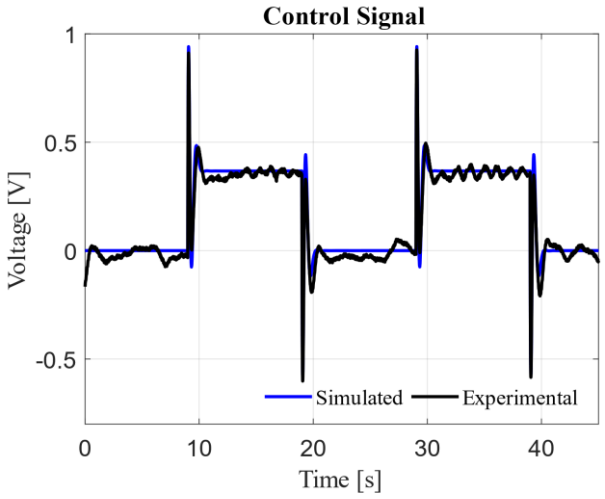

Figure 11. Control signal variation $\Delta u(t)$ computed in simulation (Simulated) and in experimental tests (Experimental).

A square wave was applied as input to the mathematical model obtained (simulation) and to the real prototype to evaluate the controller's performance in tracking the desired reference and stabilizing the system.

The results showed oscillations in the response of the real system. Still, it was possible to observe that the rise time, the error, and the control signal showed similar characteristics in both simulation and bench tests. Therefore, the methodology used was satisfactory for the case studied.

Further works intend to use other control techniques and other mathematical modeling methodologies to verify the efficiency of such procedures and compare them with the results presented in this paper.

Conflict of interest

The authors have no conflict of interest to declare.

Acknowledgements

The authors would like to thank the Instituto Federal do Paraná, Jacarezinho, and the Universidade Tecnológica Federal do Paraná, Cornélio Procópio, for their support in the development of this work.

Funding

The author(s) received no specific funding for this work.

References

Baskoro, F., & Kurniawan, F. (2020). Desain sistem pengaturan posisi sudut aero pendulum berbasis fuzzy logic controller dengan software labview. Jurnal Teknik Elektro, 9(3).

Breganon, R., Montezuma, M. A., de Souza, M. M., Lemes, R. C., & Belo, E. M. (2018). Optimal $\mathcal{H}_\infty$ controller applied to a Stewart platform. *International Journal of Advanced Engineering Research and Science*, *5*(7), 51–59. https://dx.doi.org/10.22161/ijaers.5.7.7

Doyle, J. C., Glover, K., Khargonekar, P. P., & Francis, B. A. (1989). State-space solutions to standard H/sub 2/and $\mathcal{H}_\infty$ control problems. *IEEE Transactions on Automatic Control*, *34*(8), 831-847. https://doi.org/10.1109/9.29425

Enikov, E. T., & Campa, G. (2012). Mechatronic aeropendulum: demonstration of linear and nonlinear feedback control principles with matlab/simulink real-time windows target. *IEEE transactions on education*, *55*(4), 538-545. https://doi.org/10.1109/TE.2012.2195496

Farooq, U., Gu, J., El-Hawary, M. E., Luo, J., & Asad, M. U. (2015). Observer based fuzzy LMI regulator for stabilization and tracking control of an aeropendulum. In *2015 IEEE 28th Canadian Conference on Electrical and Computer Engineering (CCECE)* (pp. 1508-1513). IEEE. https://doi.org/10.1109/CCECE.2015.7129504

Hans, S., & Ghosh, S. (2020). Position analysis of brushless direct current motor using robust fixed order $\mathcal{H}_\infty$ controller. *Assembly Automation*, *40*(2), 211-218. https://doi.org/10.1108/AA-05-2019-0084

Habib, G., Miklos, A., Enikov, E. T., Stepan, G., & Rega, G. (2017). Nonlinear model-based parameter estimation and stability analysis of an aero-pendulum subject to digital delayed control. *International Journal of Dynamics and Control*, *5*, 629-643. https://doi.org/10.1007/s40435-015-0203-0

Job, M. M., & Jose, P. S. H. (2015). Modeling and control of mechatronic aeropendulum. In *2015 International Conference on Innovations in Information, Embedded and Communication Systems (ICIIECS)* (pp. 1-5). IEEE. https://doi.org/10.1109/ICIIECS.2015.7192959

Khoirudin, M. M., & Endryansyah, E. (2020). Desain Sistem Pengaturan Posisi Sudut Aero Pendulum Menggunakan Pengendali Adaptive Neuro Fuzzy Inference System. Jurnal Teknik Elektro, 9(3), 587-595.

Mohammadbagheri, A., & Yaghoobi, M. (2011, March). A new approach to control a driven pendulum with PID method. In *2011 UkSim 13th International Conference on Computer Modelling and Simulation* (pp. 207-211). IEEE. https://doi.org/10.1109/UKSIM.2011.47

Oliveira, V., Aguiar, M., & Vargas, J. (2017). Engenharia de controle: fundamentos e aulas de laboratório. Elsevier Brasil.

Prasetyo, M. E., & Endryansyah, E. (2020). Desain sistem pengaturan posisi sudut aero pendulum berbasis pid metode genetic algorithm optimization dengan software labview. Jurnal Teknik Elektro, 9(3), 597-604.

Rigatos, G., Busawon, K., Pomares, J., & Abbaszadeh, M. (2020). Nonlinear optimal control for the wheeled inverted pendulum system. *Robotica*, *38*(1), 29-47. https://doi.org/10.1017/S0263574719000456

Rigatos, G., Siano, P., Abbaszadeh, M., Ademi, S., & Melkikh, A. (2018). Nonlinear $\mathcal{H}_\infty$ control for underactuated systems: the Furuta pendulum example. *International Journal of Dynamics and Control*, *6*, 835-847. https://doi.org/10.1007/s40435-017-0348-0

Rodrigues, R. C. S., Sombra, A. K., Torrico, B. C., Pereira, R. D., Forte, M. D. D. N., de Almeida Filho, M. P., & Nogueira, F. G. (2021). Tuning rules for unstable dead-time processes. *European Journal of Control*, *59*, 250-263. https://doi.org/10.1016/j.ejcon.2020.10.001

Sampaio, R. C., Becker, M., Siqueira, A. A., Breganon, R., de Salvi, F. B., & Belo, E. M. (2011). Model-based optimal $\mathcal{H}_\infty$ controller on the stability of a 2-dof quadrotor. In *International Design Engineering Technical Conferences and Computers and Information in Engineering Conference* (Vol. 54808, pp. 955-962). https://doi.org/10.1115/DETC2011-48447

Taskin, Y. (2017). Fuzzy PID controller for propeller pendulum. IU-Journal of Electrical & Electronics Engineering, 17(1), 3201-3207.

Tengis, T., & Batmunkh, A. (2018). Control of Single Propeller Pendulum with Supervised Machine Learning Algorithm. International journal of advanced smart convergence, 7(3), 15-22.

Thanh, P. T., Nam, D. P., Van Tu, V., Huy, T. Q., & Van Huong, N. (2019). Robust control law using $\mathcal{H}_\infty$for wheeled inverted pendulum systems. International Journal of Mechanical Engineering and Robotics Research, 8(3), 483-487.

Yoon, M. (2016). Stabilization of a propeller-driven pendulum. International Journal of Engineering Research & Technology (IJERT), 5(1), 230-233

Zhou, K., Doyle J. C., & Glover K. (1995). Robust and Optimal Control, Upper Saddle River: Prentice Hall.